Experimental and FDTD study of the EMI performance of an open-pin-field connector for modules-on-backplanes

Xiaoning Ye, Jim Nadolny[*], James L. Drewniak,
Richard. E. DuBroff, Thomas P. VanDoren, Todd H. Hubing
Electromagnetic Compatibility Laboratory, Department of Electrical and Computer Engineering
University of Missouri – Rolla, Rolla, MO 65409
* FCI Electronics, Etters, PA 17319-9769

Abstract: Experimental measurements and numerical modeling were used to study the EMI performance of a module-on-backplane connector for various configurations of signal-return pin-outs. A commercially available open-pin-field connector was used in these results to connect between the mother-board and the daughter-card. The experimental techniques, based on measuring $|S_{21}|$, included both common-mode current measurements and monopole near-field probe measurements. The FDTD method was used to provide numerical support of the near-field measurements and generally agreed with the measured results for frequencies up to *3 GHz*. The FDTD method was also used to investigate the relationship between the radiated EMI at *3 m* and the connector pin-out configurations.

I. Introduction

The module-on-backplane configuration is commonly used in high-speed digital designs. A typical module-on-backplane structure has an appreciable electrical size and, when provided with suitable excitation, can function as an unwanted EMI antenna in the frequency range of several hundred MHz into the GHz range. An appreciable signal return impedance at the connector provides the excitation for the structure as an EMI antenna [1], [2]. Connector performance, in an EMI context, can be characterized in several ways, including transfer impedance measurements [3], [4]; radiation measurements in a TEM cell or a chamber [5]; or using a common-mode current measurement technique [2], [6].

"Pin-and-box" type of connectors used on module-on-backplane connectors can result in significant EMI at system clock speeds of over *100 MHz* if the signal pin and ground pin pattern are not well designed [5]. Ideally, if a connector signal pin is completely surrounded by ground pins, then the resulting emissions are similar to that from a coaxial connection, which is the best case that can be achieved. However, the number of pins is always limited in real connector applications. Therefore, understanding how the EMI performance varies qualitatively and quantitatively with the pin-outs of the signal and signal-return pins is necessary for connector designs and applications. In the first stage of this study, the common-mode current measurement technique is used because of its simplicity. A second experimental approach, using a monopole near-field probe, is then developed to reduce the influence of measurement parasitics, and to extend the frequency range over which the measurements agree well with the numerical modeling results.

II. Common-Mode Current Measurements

The common-mode current measurement technique is first briefly discussed herein. The setup of the common mode current measurement is shown in Figure 1. It is basically a two-port $|S_{21}|$ measurement using an HP8753D network analyzer. A *60 cm ×60 cm* aluminum plate is used to separate the DUT and the measuring instruments to enhance the repeatability and dynamic range of the measurement, and eliminate artifacts associated with the dressing of cables to the measuring instrument. Two SMA bulkhead through connectors are mounted on the aluminum plate to provide the signal paths through the plate. A semi-rigid coaxial cable is attached to the DUT. The cable also provides the feeding path from Port 1 of the network analyzer to the DUT. A Fischer 2000 clamp-on current probe is placed around the semi-rigid coaxial cable and connected to Port 2. The induced common-mode current on the outer-shield of the attached semi-rigid cable is then picked up by the current probe, and fed into Port 2 of the network analyzer. A specific calibration procedure is conducted to determine the relationship between $|S_{21}|$ and the magnitude of the induced common-mode current on the attached cable I_{CM} as [6],
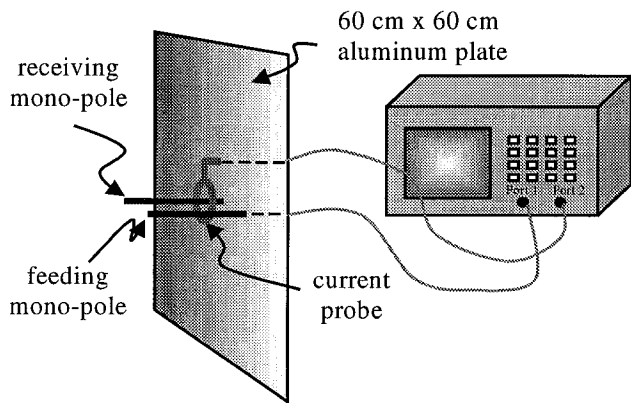
$$\left| S_{21}^{measured} \right| = \left| \frac{I_{CM} \cdot 50\,\Omega}{V_s} \right|$$

Where V_s is the driving source voltage from the network analyzer. The transfer impedance of the current probe is removed in the calibration procedure. Since the common-mode current can be readily calculated with numerical modeling, this equation makes possible an absolute comparison between the measured data and the modeled results. Other advantages of this experimental setup include its low-cost, straightforward and easy implementation, and repeatability. It can also be used for evaluation of prototype and production PCBs.
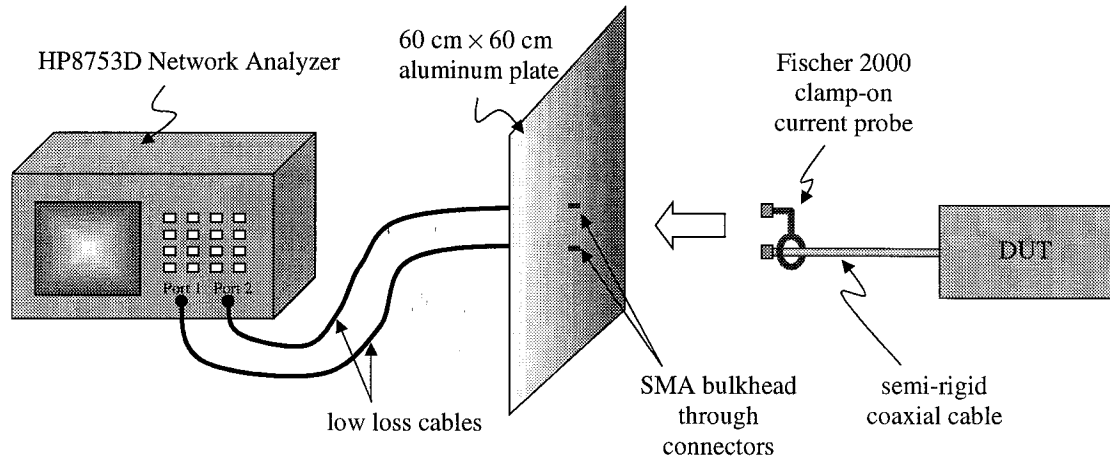
**Figure 1. Schematic representation of the experimental setup for the common-mode current measurements.**

A simple test configuration as shown in Figure 2 was built to investigate the dynamic and frequency range of this measurement technique. Two conductors with a radius of *24 mils*. were used as the feeding and receiving monopole antennas. Both monopoles were *15 cm* long, and separated by *5 cm*. The receiving monopole was directly connected to the aluminum plate, and the induced current on the receiving monopole was measured. The measured result is shown in Figure 3, together with the FDTD modeled result. Discrepancies become prominent as the frequency increases beyond *1.5 GHz*. The discrepancies are due in part to the presence of a large current probe in the proximity of the circuit under test (which introduced measurement artifacts due to parasitic coupling, but was not included in the modeling).

daughter-card. In each case, the signal was fed from the semi-rigid cable to one of the connector pins on the mother-board. On the daughter-board, the signal, coming from the mother-board through the connector, was soldered directly to the daughter-board's ground plane. The signal return path, from the daughter-board to the mother-board, was provided by using one or more additional connector pins to connect the ground planes of the two boards. In each case, unused connector pins were isolated and did not provide electrical contact with either board.
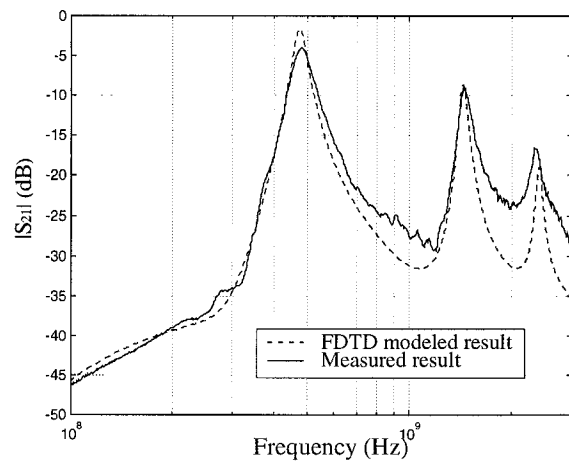
Figure 3. Modeled and measured results of the coupled monopoles.

Figure 2. Schematic of the coupled monopole antennas measurement

The common-mode current measurement described above was then applied to study the EMI performance of a module-on-backplane configuration shown in Figure 4. The dimension of the mother-board was *20 cm × 30 cm* and the daughter-board was *10 cm × 12 cm*. The extended portion of the attached *0.085"* semi-rigid coaxial cable was *20 cm*. A commercially available open-pin-field connector was used to provide various signal-return configurations between the mother-board and the

Figure 5 illustrates some possible pin-out applications of the connector in PCB designs. The ratio of the signal pins to ground pins is 1:1 for Cases A and B. In practice, there may be some compromise and the ratio will go to 2:1 or 3:1. In Case C, the ratio is 2:1. For all these pin-outs, each signal pin may have different configurations of adjacent signal-return pins. Several possible signal and signal-return pin-outs are extracted from these cases and shown in Figure 6.
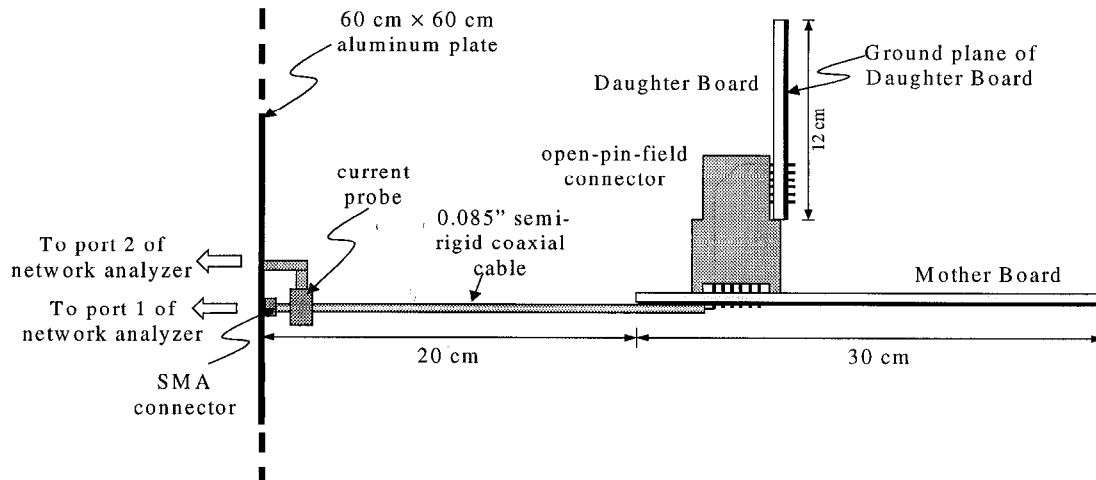
Figure 4. Setup of the common-mode current measurement of a module-on-backplane configuration
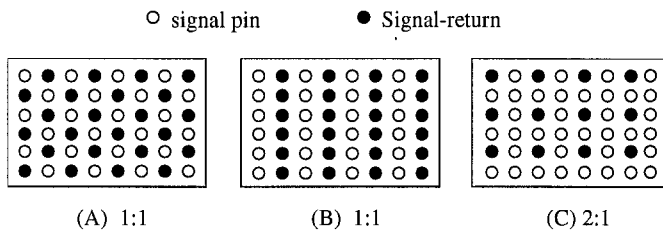
O signal pin   ● Signal-return

(A) 1:1   (B) 1:1   (C) 2:1

Figure 5. Some possible pin-out configurations.

A1   A2   A3   A4   A5
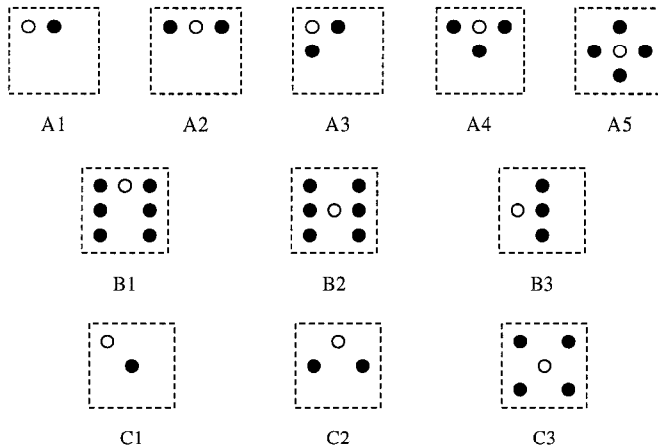
B1   B2   B3

C1   C2   C3

Figure 6. Some pin-out cases extracted from Figure 5.

Figure 7 shows the measured common-mode currents on the attached semi-rigid coaxial cable for the module-on-backplane configuration with different inter-board connections denoted as Cases A1 - A5 in Figure 6. The peaks in the common-mode current are a result of resonances of the effective radiating structures comprised of the cable, and mother-board and daughter-board planes. The results, as expected, indicate that as more adjacent ground pins are introduced, the measured common-mode current on the attached cable decreases.

However, this trend becomes less significant at high frequencies, which may be due in part to the limitation of the dynamic range of the measurement techniques and the resonance at *900 MHz*. Compared to Case A1, adding an additional ground pin on the other side of the signal pin (Case A2) results in an EMI performance improvement of approximately *6 dB*. Furthermore, the induced common-mode current for Case A5 is approximately *15 dB* less than that for Case A3, and approximately *10 dB* less than that for Case A4 at lower frequencies. Similar results can be found in [5] based on emission measurements in a TEM cell. Another observation is that Cases A2 and A3 both have two signal-return pins, and they have almost the same EMI performance at low frequencies, but case A2 is slightly better than Case A3 for frequencies above *300 MHz*. This may be due in part to the fact that Case A2 has a symmetric grounding pattern, which tends to be more beneficial for the field containment.
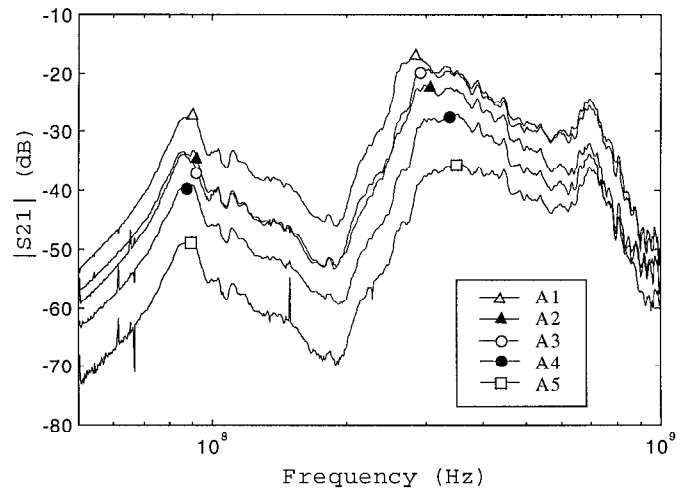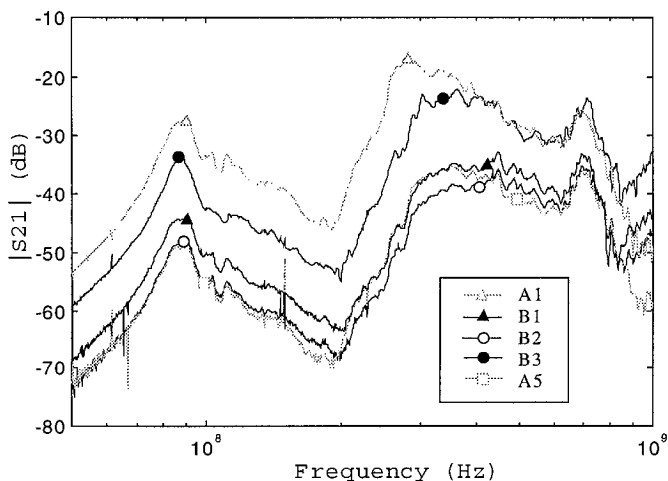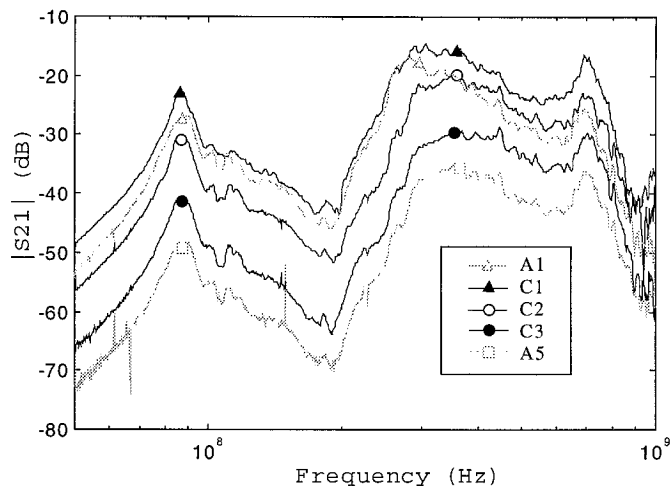

Figure 7. Measured common-mode current for the test fixture with connector pin-outs A1 – A5.

791

The measured common-mode currents for Cases B1 - B3 are shown in Figure 8. For comparison, results for Cases A1 and A5 are also shown in the same figure. The induced common-mode current for Case B2 is generally *4 - 5 dB* less than that for Case B1. This suggests that for a pin-out like Case B in Figure 5, where the signal pins are sandwiched by two columns of ground pins, the inner signal pins may induce less EMI than those at the edge. The comparison between cases B2 and B3 indicates that when the signal pin has one column of adjacent ground pins on both sides, the induced common-mode current is generally *10 -15 dB* less than that when the signal pin has only one column of adjacent ground pins. There is only slightly difference between the results of Case B2 and Case A5, which suggests that for the two different 1:1 configurations shown in Figure 5, the EMI performance of the inner pins is comparable.

Figure 8. Measured common-mode current for the test fixture with connector pin-outs B1 - B3.

The measured common-mode current for Cases C1 – C3 is shown in Figure 9. For comparison, results for Cases A1 and A5 are also shown in the same figure. The spacing between the signal pin and the nearest ground pin for Cases C1 – C3 is actually $\sqrt{2}$ times as large as that for Cases A1 – A5, while the signal-return patterns for Cases C1, C2, and C3 are the same as those for Cases A1, A3, and A5 respectively. Larger spacing between signal and signal-return pins results in a larger impedance of the signal return, and consequently, larger common-mode current is induced on the attached semi-rigid cable. Case C3 has approximately *4 - 6 dB* larger common-mode current than Case A5 due to the increase of the pin spacing.


Figure 9. Measured common-mode current for the test fixture with connector pin-outs C1 – C3.

III.   Near-Field Measurements and FDTD Modeling

While the common-mode current measurement is fairly simple to set up and produces very repeatable results, the presence of a large current probe in the proximity of the circuit under test can introduce measurement artifacts due to parasitic coupling in particular at higher frequencies. The parasitic coupling is difficult to include in numerical modeling, and this introduces difficulty in reconciling the numerical and experimental results at higher frequencies (greater than about *1.5 GHz* in this case, as shown in Figure 3). For this reason, a monopole near-field probe approach was also investigated.

The monopole near-field probe approach is schematically shown in Figure 10. In this case the mother-board was *10 cm ×* *12 cm* and the daughter-board was *8 cm × 10 cm*. Again, the signal was provided through a semi-rigid coaxial cable and then fed from the mother-board, through the connector, to the daughter-board. The signal was then routed to the daughter-board's ground plane and returned to the mother-board's ground plane through one or more signal-return pins. The near-field probe was constructed by extending the center conductor of a second semi-rigid coaxial cable *3 cm* through the mother-board. The outer shield of both coaxial cables was soldered to the mother-board's ground plane with a *360* degree connection. Ferrite sleeves were placed around both semi-rigid cables and RF absorbing materials were used to reduce the effect of parasitic coupling paths associated with the feed structure.   Port 2 of the HP 8735D network analyzer was connected to the end of the probe cable and $|S_{21}|$ results for the experimental measurements were compared with the results of FDTD modeling for two signal-return pin configurations corresponding to Cases A1 and A2 in Figure 6.
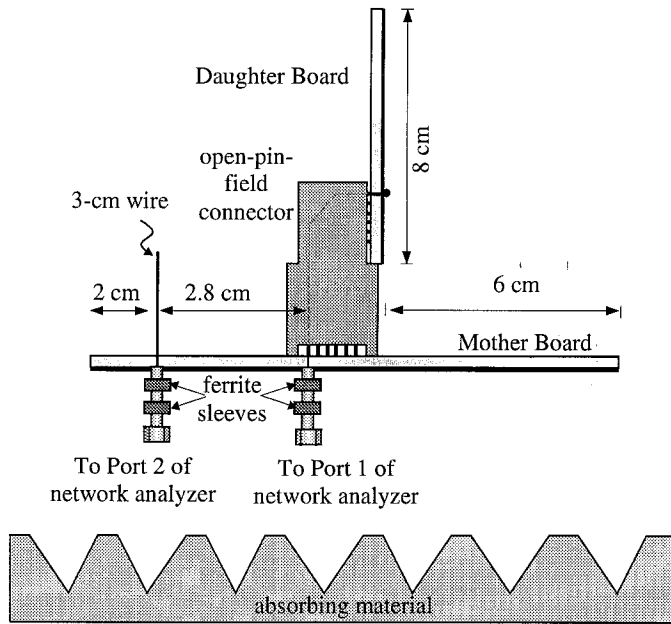
Figure 10. The experimental setup for the near-field measurement.

The FDTD modeled results and the measured results are shown in Figure 11. In the FDTD modeling, the mother-board and daughter-board were both modeled as perfect electric conductors. The actual connector pin had two 135-degree bends (as indicated by the dotted lines in Figure 10). In the modeling, the connector pin was approximated as a thin wire with a single 90-degree bend. The dielectric of the plastic housing of the connector was included in the modeling, but the dielectric of the 31-mil. thick boards was not included. A thin wire algorithm was used to model the wire structures in the fixture [7]. Eight perfectly matched layers (PML) were placed at each boundary plane of the computational domain [8], and seven white-space layers were placed between the PML and the test fixture. There is generally good agreement between the measured and modeled results shown in Figure 11. Discrepancies at low frequencies are due, in part, to the approximation introduced by using a 90-degree bend to describe the pin geometry in the FDTD modeling. Using a single 90-degree bend to model a pin containing two 135-degree bends will cause the length of the modeled pin to be slightly over-estimated. The effective inductance associated with this pin will then be similarly over-estimated in the modeling. Specifically in the case of $|S_{21}|$, the input impedance was calculated at Port 1 and the result suggested that the peak in $|S_{21}|$ at approximately 500 MHz was due to an LC-series resonance. The capacitance of this resonance seemed consistent with the capacitance between the two boards and the inductance seemed to be the inductance of the signal return pin. Over-estimating the inductance in the FDTD modeling approach would have the effect of lowering this series resonance frequency. This effect seems to be mirrored in Figure 11 where the peak $|S_{21}|$ for the modeled results occurs

at a slightly lower frequency than the peak $|S_{21}|$ for the measurements. Meanwhile, a larger signal return inductance induces larger EMI (as stated previously), which is also indicated in Figure 11 where the modeled near field is larger than the measurements at lower frequencies.
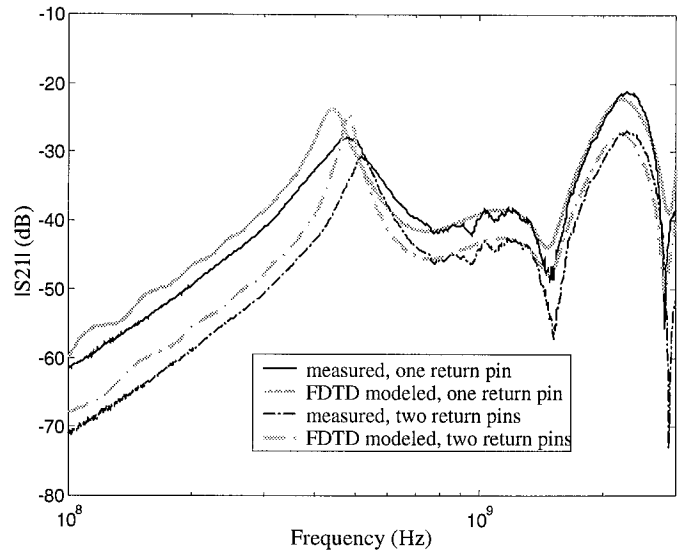
Figure 11. Comparison of measured and FDTD modeled $|S_{21}|$ for the two different connector signal return geometries: one adjacent return pin; and two adjacent return pins on opposite sides of the signal pin.

Results shown in Figure 11 suggest that the near-field EMI performance, as indicated by $|S_{21}|$, was improved by 5 to 9 dB in replacing a single adjacent signal-return pin with a pair of adjacent signal-return pins on either side of the signal pin. The difference is close to the approximately 6 dB difference in the common-mode current measurement. In order to relate this result to the radiated EMI performance, the FDTD modeling was used to calculate the radiated electric field at a distance of 3 meters from the structure. The radiated far-zone field was obtained by applying equivalence theory to the FDTD modeling results. Specifically, the FDTD method was used to calculated the electric and magnetic fields on a virtual surface, S', completely surrounding the FDTD model of the test fixture. From the calculated values of the electric and magnetic fields on this surface, equivalent magnetic and electric surface current distributions were determined. The far-zone electric field components were then calculated from these equivalent current distributions through S'. The modeled results show that the radiated field broadside to the daughter-board is larger than that broadside to the mother-board for the geometry, and corresponded to E_y polarization, as shown in Figure 12. The modeled electric field as plotted in this figure was normalized to a 0 dBm source. The 5 - 9 dB improvement provided by a pair of adjacent signal return pins, and observed with a near-field probe, seems to apply in the radiated field as well. This provides some justification for using the test setup

793

of Figure 10 to evaluate the EMI performance of various return-signal pin configurations.
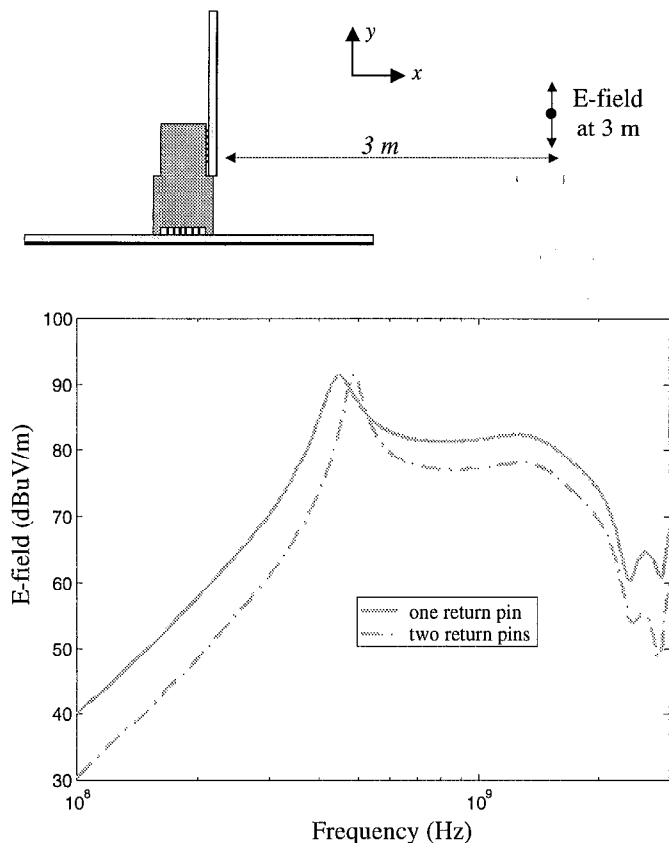

Figure 12. FDTD calculated 3 -m far field for the two signal return geometries, E_y polarization.

IV. Summary and Conclusions

A common-mode current and a near-field probe measurement technique were introduced in this study and applied to evaluate the EMI performance of an open-pin-field module-on-backplane connector. The EMI performance of the connector is very dependent on the signal-return geometry. The EMI performance can be enhanced by improving the field containment at the inter-board connection, either using multiple signal-return pins, or closer signal and signal-return spacing. Also, a symmetric signal-return designation is beneficial for EMI performance. Furthermore, routing the signal through the edges or corners of the connector pin array tends to induce more EMI than routing it through the center, since a signal pin at the center tends to have more ground pins surrounding it and achieves better field containment.

Generally, both the common-mode current and near-field probe measurement techniques are suitable for evaluating the EMI performance study of the inter-board connections, and the FDTD method is an appropriate modeling tool. The measured difference of the common-mode current (on

attached coaxial cables) between the two configurations with one or two signal-return pins at the connection is consistent with the measured difference of the near field, as well as the FDTD modeled difference of the EMI at *3 m*. The favorable agreement between the modeled and measured results presented herein indicates that the FDTD method is suitable for modeling the EMI performance of actual product connectors for frequencies into the gigahertz range.

References

[1] D. M. Hockanson, J. L. Drewniak, T. H. Hubing, T. P. VanDoren, F. Sha, M. J. Wilhelm, "Investigation of fundamental EMI source mechanisms driving common-mode radiation from printed circuit boards with attached cables", *IEEE Trans. Electromag. Compat.*, vol. 38, no. 4, Nov. 1996, pp 557-565.

[2] X. Ye, J. Nadolny, J. L. Drewniak, T. H. Hubing, T. P. VanDoren, D. E. DuBroff, "EMI associated with inter-board connection for module-on-backplane and stacked-card configurations", *IEEE Int. Symp. Electromag. Compat.*, Seattle, 1999, pp 797-802.

[3] L. O. Hoeft, J. L. Knighten, and M. Ahmad, "Measured Surface Transfer Impedance of Multi-Pin Micro-D Subminiature and LFH™ Connector Assemblies at Frequencies up to 1 GHz", *IEEE int. Symp. On Electromag. Compat.*, Seattle 1999, pp 577-582.

[4] B. Vanlandschoot, L.Martens, L. Van den Torren, D. Morlion, "An Improved Triaxial cell for transfer impedance measurements on multipins backplane connectors", *IEEE int. Symp. on Electromag. Compat.*, 1997, pp 141-144.

[5] L. K. C. Wong, "Backplane connector radiated emission and shielding effectiveness", *IEEE int. Symp. on Electromag. Compat.*, 1992, pp 346-351.

[6] D. M. Hockanson, X. Ye, J. L. Drewniak, T. H. Hubing, T. P. Van Doren, and R. E. DuBroff, "FDTD and experimental investigation of EMI from stacked-card PCB configurations," to appear in *IEEE Trans. Electromag. Compat.*

[7] A. Taflove, "The Thin Wire", Chapter 10 in *Computational Electrodynamics: The finite-difference time-domain method*, Artech House Publishers, Boston-London, 1995.

[8] J. P. Berenger, "Perfectly matched layer for the absorption of electromagnetic waves," *J. Comput. Phys.*, vol. 114, pp 185-200, Oct., 1994.

[9] M. Li, J. Nuebel, J. L. Drewniak, R. E. DuBroff, T. H. Hubing, T. P. Van Doren, "EMI from cavity modes of shielding enclosures - FDTD modeling and measurements", to appear in the *IEEE Trans. Electromag. Compat.*

[10] M. Li, S. Radu, J. Nuebel, J. L. Drewniak, T. H. Hubing, T. P. VanDoren, "Design of air flow aperture arrays in shielding enclosures", *IEEE Int. Symp. Electromag. Compat.*, Denver, 1998, pp 1059-1063.